ChemElectroChem

Research Article
doi.org/10.1002/celc.202300708

Chemistry Europe
European Chemical Societies Publishing

www.chemelectrochem.org

Diffusion Models of Mass Transport for the Characterisation of Amperometric Gas Sensors

L. Saunders,[a] L. K. Mudashiru,[b] R. Baron,[c] and B. R. Horrocks*[a]

A diffusion model for the analysis of chronoamperometric data in response to a concentration step is developed for amperometric gas sensors. This analysis avoids the difficulties with standard potentiodynamic measurements at the large specific area, high capacitance electrodes employed in these sensors. Despite the fact that typical devices comprise multiple layers with varying thicknesses and diffusivities, we show that typical chronoamperometric traces can be fitted to a simple diffusion model with a single parameter $\tau = \frac{L^2}{D}$ where L is an overall effective thickness of the diffusion barrier and D is an effective diffusion coefficient. Through a comparison of the transient and steady-state current, independent estimates of L and D in the devices can be made. The model is also extended to cover cases with interfacial kinetic barriers; such kinetic limitations lead to a change in the effective values L and D, but the simple diffusion model remains a good fit to the data. This analysis shows that transient sensor responses can be characterised by a single parameter τ and conversely that deviations from this regression model cannot be assigned to (i) complex layer architectures or (ii) interlayer kinetic barriers. Instead, we show that non-uniform accessibility effects arising from a distribution of diffusion rates across the device lead to deviations from the simple regression model, but that they may be captured approximately by a more complex model in which τ has a probability distribution.

1. Introduction

Amperometric sensors are amongst the most widely used technologies for the detection of gaseous analytes in environmental[1–5] and industrial safety applications.[6,7] They show a number of favourable performance characteristics: linearity, dynamic range, low cost, low power consumption and simplicity of operation. Alternative technologies based on spectroscopic or solid-state electronic devices have higher power consumption because of the requirements of the light source or the need for on-chip heating of the oxide semiconductor.[7,8] These characteristics and their portability make amperometric devices the dominant choice for workers in confined spaces and domestic carbon monoxide detection. They also find use in unmanned aerial vehicles.[9] The field has been reviewed in depth.[10–13] The linearity of amperometric devices is a consequence of the diffusive nature of mass transport to the underlying electrode and typical dynamic ranges are from 1 ppm to 1000 ppm. However it should be noted that ppb levels of some gases can be detected, which facilitates low-cost air quality monitoring.[1] Amperometric devices are now available for a wide range of analytes (including, but not limited to CO, NO_2, SO_2, H_2S, HCN, O_2, Cl_2), however imperfect selectivity compared to other technologies remains an issue.[7] Finally, membrane-based gas sensors for blood-gas determination in a clinical setting are well-established.[14,15]

Figure 1 shows a schematic of the construction of a typical amperometric gas sensor. The device is a three electrode system in which each electrode is a layer in the stack. The topmost electrode is the working electrode, the reference electrode is the middle layer and the counter (auxiliary) electrode is the bottom layer. These electrodes typically comprise beds of metallic nanoparticle electrocatalysts with metal foil contact strips. Each electrode layer is insulated from the electrode below by separator layers and the whole assembly, apart from the gas diffusion layers (filter + membrane), is wetted by the electrolyte. The working electrode is formed by pressing the nanoparticles against a gas-diffusion membrane. This membrane is typically hydrophobic so that the liquid electrolyte does not penetrate deeply into it and the analyte diffuses through the membrane in the gas phase. The analyte may then cross a thin liquid layer before the faradaic sensing reaction occurs at the metal nanoparticles. Additional layers on top of the membrane may include filters to chemically remove interfering species, e.g., permanganate adsorbed on SiO_2 is used to remove H_2S which can act as a poison for the Pt electrocatalyst of CO sensors.[16]

Most amperometric devices are operated with the working electrode biased to a potential at which the oxidation or reduction of the analyte occurs at the potential-independent mass transport-limited rate. This renders the sensor output less susceptible to effects of slow drift of the reference potential.

[a] L. Saunders, B. R. Horrocks
School of Natural and Environmental Sciences, Bedson Building, Newcastle University, Newcastle upon Tyne, NE1 7RU (UK)
E-mail: ben.horrocks@ncl.ac.uk

[b] L. K. Mudashiru
Durham University, Stockton Road, Durham, DH1 3LE (UK)

[c] R. Baron
Alphasense, Sensor Technology House, 300 Avenue West, Skyline 120, Great Notley, Essex CM77 7AA (UK)

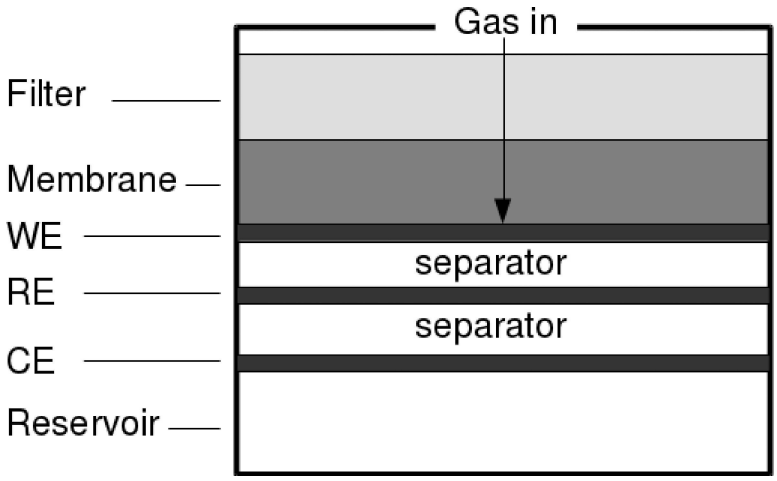

Figure 1. Schematic diagram of a typical amperometric gas sensor. The influx of the analyte may be controlled by a constriction/headspace, it may then pass through a chemical filter layer to remove interferents/catalyst poisons before entering the gas-diffusion membrane and finally an electrolyte layer wetting the catalyst layer on the working electrode, WE. Below the WE are the reference and counter electrode layers (RE, CE) and an electrolyte reservoir.

The sensor signal is simply the transport-limited current which is mainly controlled by diffusion of the analyte through the various layers of the device between the inlet and the working electrode. The important metrics for a device include the sensitivity (nA/ppm) which is the slope of the linear portion of the calibration plot, the linear range and the response time.[17,18] The response time is typically reported as the time required to obtain 90% of the steady state current in response to a step change of analyte concentration from zero to a fixed level. This parameter, t_{90}, is determined by the thickness of the various layers in the device (L_i) and the diffusion coefficients (D_i) of the analyte in these layers. In principle, the values of L_i and D_i could be obtained by standard electrochemical experiments, e.g., by analysing the chronoamperometric response to a potential step using appropriate modifications of the Cottrell equation.[19] However, the differential capacitance of the nanoparticulate working electrodes is so large (order of 10^{-1} F) that the faradaic current cannot be separated from the double layer charging current, i.e., $RC \gg t_{90}$ for typical devices. Cyclic voltammetric measurements are also of little utility because even at scan rates as low as 0.1 $mV\,s^{-1}$ the capacitive background is too large: $i_{bck} \simeq 10\,\mu A$, which is of a similar order to the sensor output for 150 ppm analyte. Potentiostatic measurements are therefore necessary.

Information has been obtained by analysing the dependence of the steady-state transport-limited currents on device construction and layer thicknesses.[20,21] This approach was used to estimate the contribution of the various diffusion barriers to the sensor signal, but it does not provide individual values of L and D. The current fluctuations in amperometric gas sensors have also been analyzed and the noise spectra may be correlated to the state of the device.[22] However, the precise

L. Saunders: Dr. Luke Saunders received his PhD from Newcastle University. His PhD work was based upon characterising mass transport in electrochemical gas sensors. He has worked within the battery manufacturing industry on the degradation characteristics of Li-ion batteries and is currently investigating electric motor technology.

R. Baron: BSc, MSc Brest University, PhD ENSCR, HDR University of Lyon. Postdoc at HUJI and Oxford. Joined Alphasense Ltd part of AMETEK in 2009, presently Technical Director. Research interests in electrochemistry and gas sensing.

L. K. Mudashiru: BSc, MSc, PhD, MBA at Newcastle University, UK, previous member of research groups at Newcastle University and University of Calgary, Canada. Joined Durham University in 2004 and now Deputy Head of International Student Recruitment. Still maintain interests in electrochemistry and nanoscience.

B. R. Horrocks: BSc and PhD at Imperial College London, member of academic staff at Newcastle University since 1994. Research interests in electrochemistry and nanoscience.

origin of $1/f^{\alpha}$ noise is often unclear. In this report we develop a simple diffusion model for the response of an amperometric gas sensor to a step-change in analyte concentration and discuss its uses and limitations. This approach facilitates a quantitative analysis of amperometric gas sensor transient performance and we show that effective values of L and D can be estimated by comparing the transient and steady-state responses. We find that the values of D vary with temperature as $D \sim T^{1.75}$ for a commercial CO sensor.[23] Finally, deviations of the response of the device from the simple model are shown to be consistent with a model based on distributed mass transport.

Experimental Section

Amperometric sensors were supplied by Alphasense Ltd. CO-AF refers to the standard device with nanoparticulate Pt working, reference and counter electrodes. Full details are available at www.alphasense.com/index.php/products/carbon-monoxide-safety/. In brief, the electrodes are in the form of a stack; the working electrode is at the top, next to the gas-permeable PTFE membrane and the counter and reference electrodes are in lower layers. The working electrodes comprise a Pt black electrocatalyst pressed onto a sheet of microporous PTFE membrane. Electrical contact is provided by a strip of Pt foil. The electrolyte is 5 M H_2SO_4.

Three different types of CO sensors were studied in this work: "standard", "thick membrane" and "without filter". The standard design uses a PTFE membrane of pore diameter 9–12 μm, a porosity of 40–45 % and a thickness of 0.18 mm. Some sensors were prepared using a thicker PTFE membrane, which has a porosity of 20 % and a thickness of 0.25 mm. Both standard and thick membrane designs employ a filter layer of potassium permanganate adsorbed on silica on top of the PTFE membrane. This filter layer removes possible interferents and catalyst poisons such as H_2S. The devices described as "without filter" are standard designs with the filter omitted leaving a gas space in the same form factor.

2000 ppm CO in zero air was obtained from BOC Industrial Gases Ltd. This was mixed with zero air (BOC, 270020-V) in various proportions to produce CO concentrations in the range 0–1000 ppm. Zero air is prepared by mixing pure oxygen and nitrogen in a 1:4 ratio and has a much lower level of impurities than ambient air (hydrocarbons $<$ 0.1 vpm; $CO_2 < 1$ vpm; $H_2O < 2$ vpm and NOx $<$ 0.1 vpm). Volume flow rates of the gases were controlled using digital mass flow controllers (Brooks, 5850S) using the Brooks 0260 Smart Interface and software. The mass flow controllers have a settling time of $\simeq$ 1 s, which is much shorter than the 90 % response time t_{90} of the CO-AF devices. The sensor test system comprised 6 mm id PVC tubing and manual valves to deliver the gas to the sensors mounted on a PCB board (Alphasense). The sensors were covered with a tightly-fitting PVC hood (Alphasense) mounted on the PCB board in order to minimize the dead volume in the system.

Some temperature-dependent measurements were carried out at Alphasense Ltd on a similar system with temperature control provided by a Climatic environmental chamber. The system, comprising tubing, sensor, gas hood and electronic board, was stabilized for two hours at a chosen temperature in the chamber before the gas exposure step. Typically, the test consisted of exposing the sensor to a flow of zero air for 5 min, then to a flow of CO at 400 ppm for 10 min and finally to a flow of zero air for 10 min. The CO used in these experiments was from a certified bottle of 2500 ppm CO in zero air (Air Products, UK). The air used both for the baseline and the gas dilution corresponds to a 'zero air' obtained from an air purification system. The air purification system included a thermal dryer, a heated Platinum scrubbing bed (Parker HPZA-18000-220 Zero Air Generator), particulate filters and final chemical scrubbing. A flow rate of 0.5 L min^{-1} was used for all these experiments.

Chronoamperometric measurements at low sample rates were carried out using a proprietary potentiostatic PCB board which operates at a fixed dc bias of 0.0 V against the device reference (Alphasense) and samples the current at intervals of 1 s. In cases where higher time resolution or variable dc bias was required, a PalmSens 3 potentiostat was connected to the board and the sampling interval was decreased to about 28 ms. Impedance spectra were also recorded using the PalmSens instrument. The data collection and software control of the gas flow were implemented via USB connection to a laptop computer under MS Windows 7.

2. Simulation models

An amperometric gas sensor (Figure 1) has at least two distinct diffusion barriers, the gas membrane and the electrolyte. In this section we first describe a two-layer model including two phases (1, 2) which in a specific case might represent gas phase and liquid phase diffusion. It can be extended in a straightforward fashion to models with more layers and in section 2.4 we consider the case where the diffusion coefficient has an arbitrary dependence on distance. In the following sections we show that the response of complex models is often well-described by a single characteristic time τ and this may be obtained by regression analysis of the data or estimated by analytical approximations.

2.1. Two-layer Model

Below, k is the heterogeneous rate constant for interfacial transfer of the analyte from the outer phase phase (2) into the inner phase (1). K is the partition coefficient between phases (1) and (2) and D_2 and D_1 are the diffusion coefficients in phases (1) and (2). L_1 and L_2 are the thicknesses of the phases with the liquid phase next to the electrode at $0 < z \leq L_1$ in a typical case.

The chronoamperometric response of such a sensor may be modeled by three different processes at different distances, z from the electrode surface: gas-phase diffusion for the region ($L_1 < z \leq L_1 + L_2$),

$$D_2 \frac{\partial^2 c_2}{\partial z^2} = \frac{\partial c_2}{\partial t} \tag{1}$$

the kinetics of transfer of the analyte from the outer phase (2) into the inner phase (1),

$$D_2 \left.\frac{\partial c_2}{\partial z}\right|_{z\to L_1^+} = kc_2 - \frac{k}{K}c_1 = D_1 \left.\frac{\partial c_1}{\partial z}\right|_{z\to L_1^-} \quad (2)$$

and the diffusion of the analyte in the liquid electrolyte ($0 < z \le L_1$),

$$D_1 \frac{\partial^2 c_1}{\partial z^2} = \frac{\partial c_1}{\partial t} \quad (3)$$

the initial conditions are simply:

$$c_1(z,\ 0) = 0; \quad 0 < z \le L_1 \quad (4)$$

$$c_2(z,\ 0) = 0; \quad L_1 < z \le L_1 + L_2 \quad (5)$$

and the boundary conditions are:

$$c_1(0,\ t) = 0 \quad (6)$$

$$c_2(L_1 + L_2,\ t) = c^* \quad (7)$$

which express the fact that the reaction is insensitive to the electrode kinetics at the usual operating potential of the sensor and the concentration at the sensor surface rises abruptly from zero to a constant value c^* for $t \ge 0$. The model was solved using a standard 3-point finite difference scheme with second order, centered spatial derivatives, but fully implicit in time. The concentration profile in the gas phase was discretized on a grid of 100 uniformly-spaced points and another, similar spatial grid was used for the liquid phase.

2.2. Single Diffusion Barrier

Before we discuss solutions of the full model Eqs. (1–7), it is useful to consider the simpler case of diffusion through a single barrier of thickness L with diffusion coefficient D. This applies when one of the diffusion barriers in the full model is rate-determining. The calculation that follows is for the typical experiment in this work, where a fixed electrode potential is applied that drives the electrode reaction at the mass transport limited rate and a jump in analyte concentration is made by opening the gas line which supplies the analyte (CO in zero air). In such an experiment, the analyte concentration at the external sensor surface is initially zero and is then abruptly stepped to a value c^* determined by the mixing ratio of the analyte and zero-air gas lines. We make the approximation that this concentration step is instantaneous, which is equivalent to the assumption that the concentration profile of the analyte reaching the external membrane surface is sharp.

The time taken for the gas to travel between the mixing point and the sensor leads to diffusional broadening of the analyte profile. The width of the concentration profile $W \sim \sqrt{D\frac{V_{dead}}{V_f}}$ where V_{dead} and V_f are the dead volume and the volume flow rate. If the area of cross section of the tubing is A, this broadening can be neglected when the time $\frac{WA}{V_f}$ is much less than the sensor response time τ defined below. For typical experimental values $D \simeq 0.1\ cm^2 s^{-1}$; $A \simeq 0.3\ cm^2$; $\frac{V_{dead}}{V_f} \simeq 2\ s$ and $V_f \ge 8\ cm^3 s^{-1}$ then $\frac{WA}{V_f} \le 0.016\ s$ and the assumption is reasonable for all the experiments in this paper.

Under this assumption, the experiment corresponds to a concentration step at a membrane-covered electrode[15,24] and a similar model has been applied to an amperometric oxygen sensor.[25] In the model of Figure 2, partition equilibria and kinetics between the membrane phase and electrode or external sample are ignored, but these effects will be

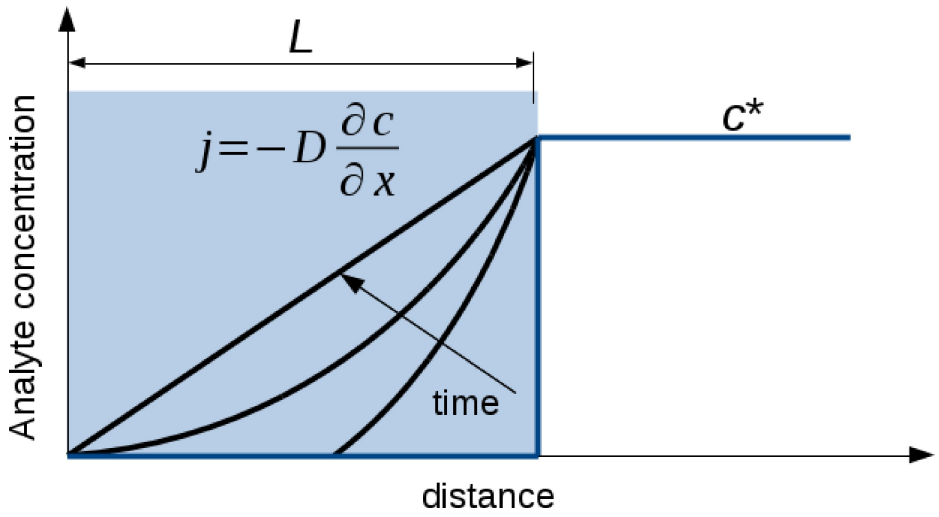

Figure 2. Schematic diagram of a concentration step experiment at a membrane-covered electrode. The y-axis is the analyte concentration. At $t = 0$, the concentration profile is given by the blue line. The initial concentration is zero everywhere and jumps instantaneously to a value c^* for $t > 0$ outside the membrane. Inside the membrane, the concentration profiles evolve with time (black curves = $c(z,t)$) until a steady-state is reached as $\frac{Dt}{L^2} \to \infty$ in which the profile is linear from c^* at the external surface of the membrane ($z = L$) to zero at the electrode surface ($z = 0$).

introduced using the full model of section 2.1, Eq. (2) and treated in section 3.6.

The single layer model is described by the evolution with time and coordinate normal to the electrode (z) of the concentration profile $c(z,t)$ according to the diffusion equation.

$$D\frac{\partial^2 c}{\partial z^2}=\frac{\partial c}{\partial t} \tag{8}$$

Subject to the initial condition $c(z,\ t)0$ for $z<L$ and $c(z,\ t)=c^*$ for $z>L$ and the boundary conditions $c(0,\ t)=0$ and $c(L,\ t)=L$ for $t>0$. The solution of this model in terms of the Laplace transforms of the concentration and of the flux $\bar{j}$ is straightforward and is given by Eq. (9):

$$\bar{j}=\frac{D}{L}\left[\frac{c^*}{\sqrt{s}\sinh\sqrt{s}}\right] \tag{9}$$

where s is the Laplace parameter corresponding to the dimensionless time $\tau=\frac{Dt}{L^2}$ and the flux $j=-D\frac{\partial c}{\partial z}\Big|_{z=0}$. The Laplace transform in Eq. (9) is easily inverted[26] to give the current transient in equation Eq. (10).[24]

$$\frac{i}{nFA}=j=D\frac{c^*}{L}\left[1-2\Sigma_{n=1}^{\infty}(-1)^{n-1}e^{-n^2\pi^2\frac{t}{\tau}}\right] \tag{10}$$

Below we refer to $\tau=\frac{L^2}{D}$ as the characteristic time. It is simply related to the time to reach 90% of the sensor response, $t_{90}\simeq 0.3\tau$, a common metric for sensor performance. The chronoamperometric response when the gas is switched off, i.e., when the concentration at the outer membrane surface returns abruptly to zero, is obtained simply by subtracting the bracket in Eq. (10) from unity. The full concentration profile which describes the black curves of Figure 2 is also known[26] and is given by Eq. (11).

$$\frac{c(z,\ t)}{c^*}=\frac{z}{L}-2\Sigma_{n=1}^{\infty}\frac{(-1)^{n-1}}{n\pi}e^{-n^2\pi^2\frac{t}{\tau}}\sin\frac{n\pi z}{L} \tag{11}$$

Eq. (10) is used as the basic regression model for the analysis of experimental data in this paper and also to obtain effective characteristic times by fitting to more complex models. It was fitted to experimental data by the method of least squares using a standard Levenberg-Marquardt algorithm.[27] Sufficient precision for the evaluation of the current transient was obtained by direct summation of the first 40 terms of the series, except at $t=0$ where the sum was simply set to a value of $\frac{1}{2}$. Although it is derived for an oversimplified model of real amperometric gas sensors, Eq. (10) gives a satisfactory fit to much experimental data for the reasons discussed in subsequent sections.

2.3. Approximate solutions for a two-layer model

A more realistic model of the current response of an amperometric device to a concentration step involves two diffusion barriers with diffusion coefficients D_1 and D_2 representing diffusion in a region of thickness L_1 and in a second region of thickness L_2. However, as demonstrated below, the shapes of the chronoamperometric responses for the two-layer model are very similar to those of the single layer model of the previous section. This suggests that it should be possible to approximate the numerical solution of the two-layer model using the single layer Eq. (10) as long as it is understood that the values of D and L should be considered an *effective* diffusion coefficient and an *effective* thickness which combine the values of the four actual parameters of the model (D_1, L_1, D_2, L_2). Previous workers have also noted that amperometric sensors may be described by an effective diffusion time L^2/D.[17]

First, we consider the current a long time after the concentration step when it has reached a steady-state value. It is straightforward to see that the steady-state current as $\frac{t}{\tau}\rightarrow\infty$ must be determined by a mass transport coefficient $\frac{D}{L}$ that is given exactly by:

$$\frac{L}{D}=\frac{L_1}{D_1}+\frac{L_2}{D_2} \tag{12}$$

as long as the electrode is uniformly accessible. In that case, the overall flux j will be limited by whichever of the two barriers gives the lowest flux: $j^{-1}=j_1^{-1}+j_2^{-1}$ where $j_1=D_1\frac{c^*}{L_1}$ and $j_2=D_2\frac{c^*}{L_2}$. Eq. (12) relates D and L to D_1, L_1, D_2 and L_2. On its own, it does not allow a separate determination of D and L; this requires a consideration of the time-dependent part of the response, i.e., the factor controlled by the characteristic time $\tau=\frac{L^2}{D}$ in Eq. (10).

If the two diffusion coefficients were equal, $D_1=D_2$, then the model would be equivalent to a single layer with thickness $L=L_1+L_2$. The corresponding characteristic time $\frac{L^2}{D}$ would be $\frac{(L_1+L_2)^2}{D_1}$. This suggests an approximation for the two-layer model. If the characteristic time τ for diffusion across any layer of thickness L_i is L_i^2/D_i then we can approximate the time-dependent behaviour of the second layer by adjusting its thickness and diffusion coefficient, keeping τ fixed, until the diffusion coefficient is equal to that in the other layer. This gives an effective thickness of, $L'\simeq L_2\sqrt{\frac{D_1}{D_2}}$. Now we simply add this effective thickness to L_1, as above, to obtain the overall characteristic time: $\frac{L^2}{D}\simeq\frac{(L_1+L')^2}{D_1}$. We can approximate the two-layer chronoamperometric response by inserting $\frac{L^2}{D}$ into Eqs. (9) and (10) then we can use Eq. (12) to solve for D and L in terms of D_1, L_1, D_2 and L_2.

$$\frac{L^2}{D}=\frac{L_2^2}{D_2}+\frac{2L_1L_2}{\sqrt{D_1D_2}}+\frac{L_1^2}{D_1} \tag{13}$$

The effective values of L and D for use in Eq. (10) are therefore:

$$L = \frac{\frac{L_2^2}{D_2} + \frac{2L_1L_2}{\sqrt{D_1D_2}} + \frac{L_1^2}{D_1}}{\frac{L_1}{D_1} + \frac{L_2}{D_2}} \tag{14}$$

$$D = \frac{\frac{L_2^2}{D_2} + \frac{2L_1L_2}{\sqrt{D_1D_2}} + \frac{L_1^2}{D_1}}{\left(\frac{L_1}{D_1} + \frac{L_2}{D_2}\right)^2} \tag{15}$$

As $\frac{D_2}{D_1} \to 1$, $L \to L_1 + L_2$ and as $\frac{D_2}{D_1} \to \infty$, $L \to L_1$ and $D \to D_1$ as expected.

Figure 3 shows a series of simulations of the full model, Eqs. (1–7), and the fit of the simple regression model of Eq. (10). It is clear that the existence of multiple layers does not dramatically change the shape of the chronoamperometric response when the diffusion coefficient ratio varies over two orders of magnitude. This is the basic justification for using equation (10) as the regression model for experimental data in subsequent sections. Figure 4 compares the effective values of L and D estimated by the regression model displayed in Figure 3 to those calculated by the approximations in Eqs. (14) and (15). The effective diffusion coefficient is reasonably well described over a wide range of D_1/D_2 ratios by Eq. (15) although the effective thickness approximation of Eq. (14) is not as good.

2.4. Distance-dependent diffusion coefficient

The nature of the diffusion barriers in a working amperometric gas sensor may be much more complex than a two-layer configuration. As well as diffusion in the liquid electrolyte phase or through the porous membrane, it is possible that the manufacturing process can affect the membrane porosity or cause partial flooding of the membrane by the electrolyte. In general, therefore, even a single membrane may not present a simple diffusion barrier to the analyte and the appropriate model for the sensor may include a distance-dependent diffusion coefficient:

$$\frac{\partial}{\partial z} D(z) \frac{\partial c}{\partial z} = \frac{\partial c}{\partial t} \tag{16}$$

Eq. (16) was solved by an implicit finite difference method after discretization as indicated in Figure 5. The labels $i-1$, i, $i+1$ indicate generic lattice points spaced by a distance Δ and the values of concentration and diffusion coefficient at each lattice point are labelled c_i and D_i. The difference equations were obtained by calculating the fluxes j', j centered at the midpoints indicated by the dashed lines and using the appropriate average diffusion coefficient $\frac{1}{2}(D_{i+1} + D_i)$ or $\frac{1}{2}(D_i + D_{i-1})$.

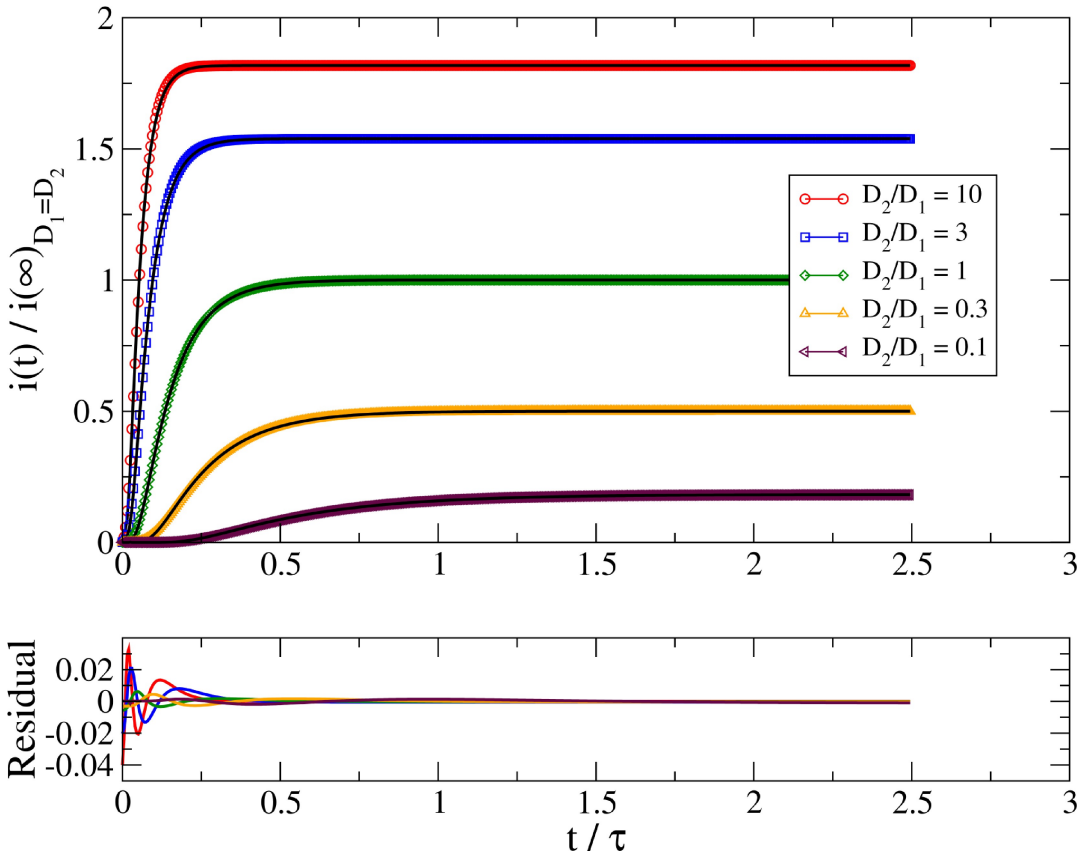

Figure 3. The chronoamperometric response (symbols) of the two-layer model of Eqs. (1–7) and the fit of the regression model based on a single-layer (lines) and Eq. (10). The simulation parameters for the two-layer model were: $L_1 = L_2 = 0.5$ cm, $D_1 = 1$ cm^2 s^{-1}, $K = 1$ and $dt/\tau = 5\times10^{-3}$. The rate constant k was set to 10^6 cm s^{-1}, sufficient to ensure the currents were purely diffusion-controlled. The currents are normalized to the steady-state current for the case $D_1 = D_2$.

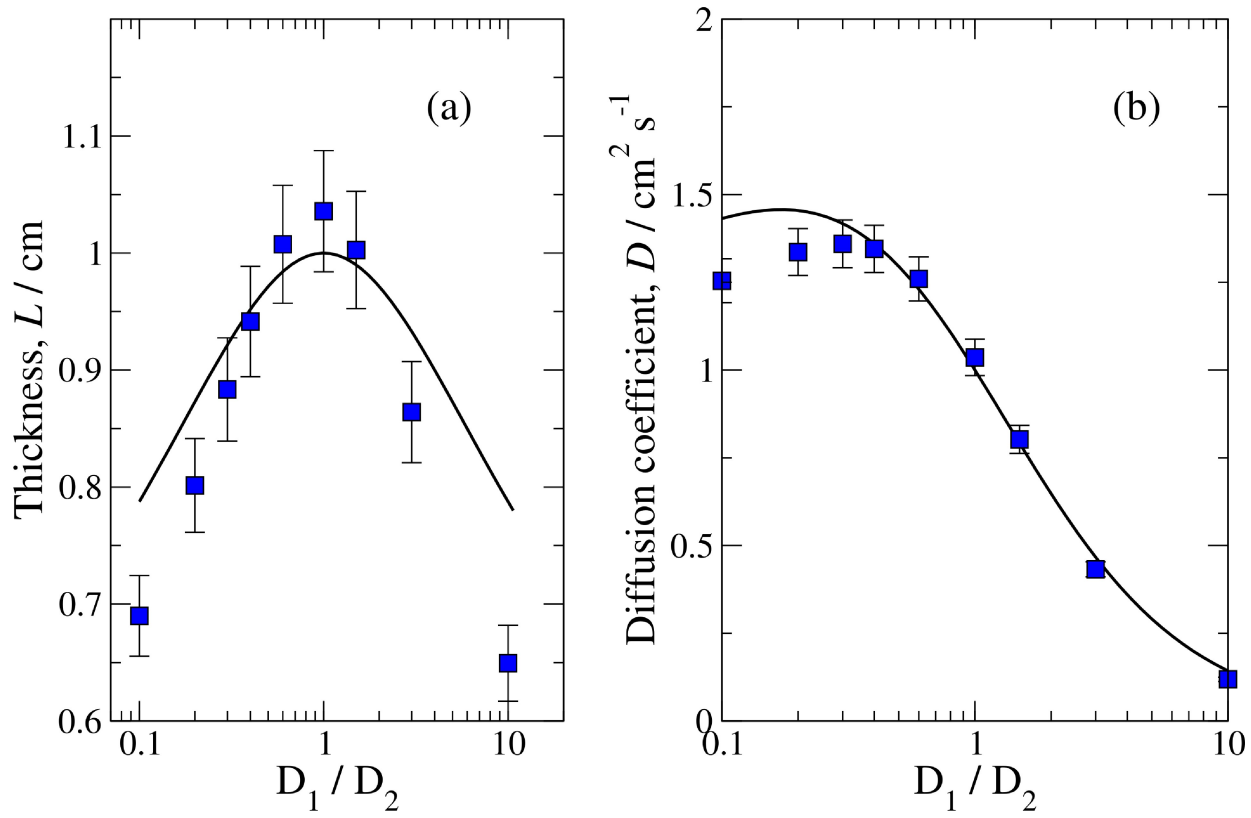

Figure 4. Comparison of two different estimates of effective thicknesses L and effective diffusion coefficients D for a two-layer diffusion model defined by Eqs. (1–7). The simulation parameters for the two-layer model were: $L_1 = L_2 = 0.5$ cm, $D_1 = 1$ cm^2 s^{-1}, $K = 1$, $k = 10^6$ cm s^{-1} and $dt/\tau = 5\times10^{-3}$. The symbols are the estimates obtained from the regression model of Eq. (10). The solid lines are the estimates based on the closed form approximations of Eq. (14) and Eq. (15). (a) Effective thickness L; (b) Effective diffusion coefficient D.

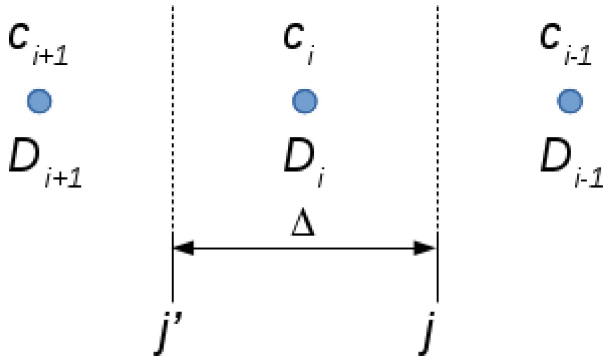

Figure 5. Discretization of the concentration (c_i, c_{i+1}, …) and diffusion coefficient (D_i, D_{i+1}, …) for the solution of Eq. (16). The distance between lattice points $i-1$, i, $i+1$ is Δ.

$$\frac{\partial j}{\partial z} = \frac{j' - j}{\Delta} = \frac{\Delta c}{\Delta t} = \frac{1}{2\Delta^2}[(D_{i+1} + D_i)(c_{i+1} - c_i) - (D_i + D_{i-1})(c_i - c_{i-1})] \quad (17)$$

The equations to be solved are therefore:

$$c_i^{t+1} - c_i^t = \frac{\Delta t}{2\Delta^2}\left[(D_{i+1} + D_i)c_{i+1}^{t+1} - (D_{i+1} + 2D_i + D_{i-1})c_i^{t+1} + (D_i + D_{i-1})c_{i-1}^{t+1}\right] \quad (18)$$

where t, $t+1$ indicate quantities at times t and $t+1$ with time discretized in units of Δt. Eq. (18) are tridiagonal and were solved by a standard algorithm.[27]

2.5. Approximate solution in terms of an average diffusion coefficient

If we assume a region of thickness $0 < z < L$ in which the diffusion coefficient is $D(z)$ then we can calculate an effective thickness for a membrane with a constant diffusion coefficient $D = D(0)$ such that the time constant of the effective membrane is the same as that of the actual membrane by extending the analysis leading to Eq. (13). We imagine the effective membrane as a series of layers in which the diffusion coefficient is constant $D(0)$, but for which each layer thickness is adjusted according to Eq. (19) so that the value of τ is unchanged from that in the corresponding layer of the real membrane of thickness dz. The effective membrane thickness is obtained by integration of:

$$dL' = \sqrt{\frac{D(0)}{D(z)}}dz. \quad (19)$$

The characteristic time for the sensor response is then:

$$\tau = \frac{L^2}{D} = \frac{1}{D(0)}\left[\int_0^L \sqrt{\frac{D(0)}{D(z)}}dz\right]^2 \quad (20)$$

The mass transport coefficient that determines the steady-state flux, assuming uniform accessibility of the electrode, is given by an extension of Eq. (12),

$$\frac{L}{D} = \int_0^L \frac{dz}{D(z)} \quad (21)$$

Finally, the effective diffusion coefficient, D, and effective thickness, L, for the equivalent simple one-layer system are:

$$L = \frac{\left[\int_0^L \sqrt{\frac{D(0)}{D(z)}}dz\right]^2}{D(0)\int_0^L \frac{dz}{D(z)}} \quad (22)$$

and

$$D = \frac{1}{D(0)}\left[\frac{\int_0^L \sqrt{\frac{D(0)}{D(z)}}dz}{\int_0^L \frac{dz}{D(z)}}\right]^2 \quad (23)$$

Eqs. (22) and (23) reduce to Eqs. (14) and (15) when the diffusion coefficient takes the constant value D_1 in the region $0 < z \leq L_1$ and D_2 for $L_1 < z \leq L_1 + L_2$.

Figure 6 compares a finite difference simulation of a distance-dependent diffusion coefficient with the simple regression model of Eq. (10) using either the values of L and D estimated by the approximation in Eqs. (22) and (23) above or determined by least squares fitting of the regression model. Again, Eq. (10) fits well the the chronoamperometric response for the more realistic, but more complex model based on Eq. (16) with distance-dependent diffusivity. The steady-state current and the characteristic time τ are reasonably well approximated by Eqs. (22) and (23) even though the diffusion coefficient varies by two orders of magnitude across the membrane in this example.

In summary, Eq. (10) does not provide an exact description of the chronoamperometric response of models comprising multiple barriers, however in many cases the differences are sufficiently small that it can be applied to the analysis of experimental data to derive useful effective diffusion coefficients D and thicknesses L. If a new device is constructed from layers with known transient responses, then Eqs. (22) and (23) provide a useful method to predict approximate device characteristics. On the other hand, if the device construction is quite new, then its transient response is best characterised by fitting of the regression model of Eq. (10) to experimental data.

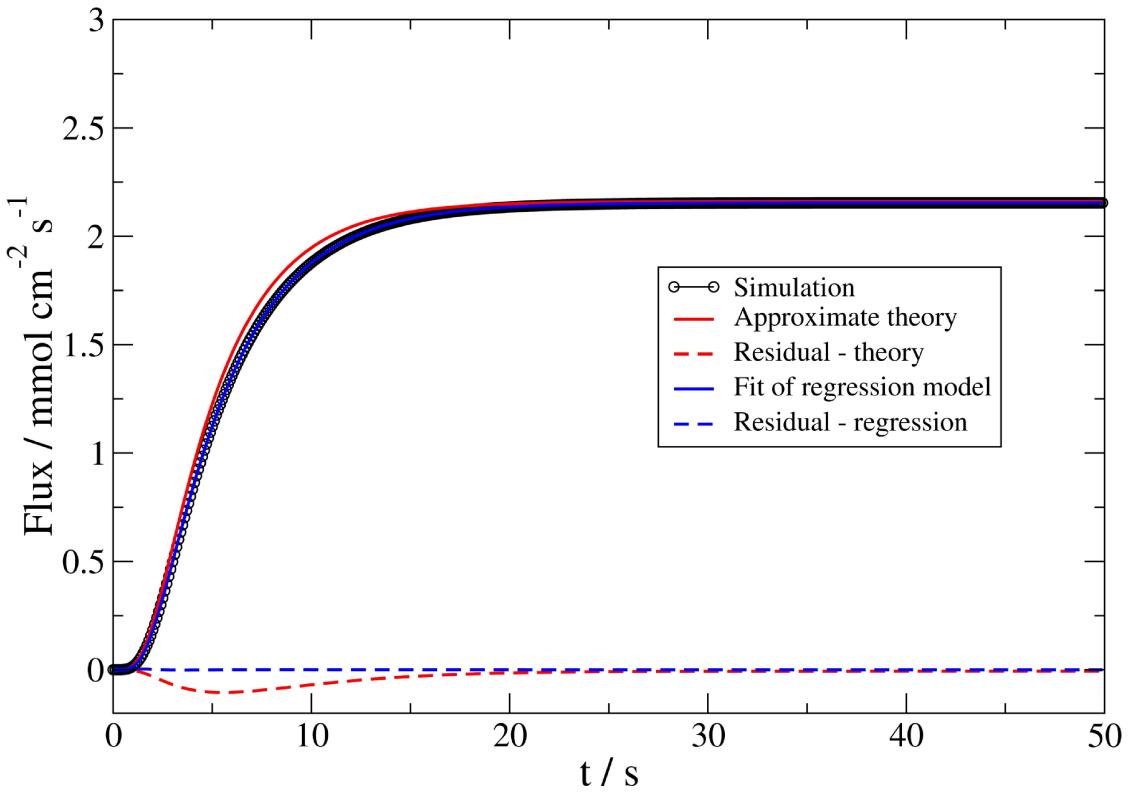

Figure 6. Simulation of the chronoamperometric response to a unit step change in concentration for a barrier of thickness $L = 0.1$ cm and distance-dependent diffusion coefficient varying linearly between $D(0) = 10^{-5}$ cm^2 s^{-1} and $D(L) = 10^{-3}$ cm^2 s^{-1}. The symbols are the result of the simulation of the full model (Eq. (16)), the red curve represents the approximate theory of Eqs. (22) and (23) using the extended Simpson's rule to evaluate the integrals and the blue curve is the fit of the regression model of Eq. (10).

3. Results and Discussion

3.1. Electrochemical characterisation of the amperometric CO sensors

Figure 7(a) shows an impedance spectrum of a standard CO AF sensor at the normal dc operating potential of 0.0 V. In order to avoid excessively large currents, the amplitude of the applied ac signal was 1 mV and the frequency range was 0.1–10 Hz. The Nyquist plot has the typical form for a porous electrode,[28,29] which may be described using a transmission line to model the pores and in the lowest frequency regime shows a simple differential capacitance $-Z'' = \frac{1}{2\pi c}$ (Figure 7(b)). The differential capacitance of the device is extremely large (0.257 ± 0.00033 F) corresponding to a wetted metal area of order 1 m^2 for a specific capacitance of 20 $\mu F\,cm^{-2}$. Even at a scan rate of 1 $mV\,s^{-1}$ the capacitive current is about 260 μA, which is much greater than the typical sensor response to 400 ppm CO of about 30 μA. This is the reason that we apply a concentration-step at a fixed dc bias and analyse the chronoamperometric response using Eq. (10) in order to investigate the electrochemical behaviour of the CO-AF devices.

In section 3.2 we discuss the typical response of CO-AF devices to a concentration step, the analysis of the data using Eqs. (9) and (10) and some limitations of the model. Then we employ this analysis to obtain effective values of *L* and *D* for "standard", "thick membrane" and "without filter" devices over a range of temperatures in section 3.4. We address the issue of non-uniformly accessible electrodes by an approximate method in section 3.5 and finally, we discuss the extent to which interfacial kinetic barriers between layers of the device can be probed by these experiments in section 3.6.

3.2. Chronoamperometric response to a concentration-step

Figure 8 shows typical chronoamperometric data for the response of a standard CO-AF device to 100 ppm CO in zero air. The blue line is the fit of Eq. (10) to the data and the red line is the residual: experiment – theory. The fit is good at both short and long times, but at intermediate times, the theoretical curve lies slightly above the experimental data. Importantly, the characteristic times obtained for a step up in concentration (47.3 s) and for the recovery as the concentration is returned abruptly to zero (45.1 s) are approximately the same, as expected for a diffusion model. Figure 9 shows similar data, but with higher time resolution (28 ms/pt) compared to Figure 8 where the current was sampled at a rate of 1 s/pt. The signal-to-noise ratio is worse because there is less averaging of the data at the higher sampling rate, but the fit of the diffusion model is still good. Figure 9(b) also illustrates an alternative method of data analysis based on the same model, but using Eq. (9) for the Laplace-transformed current. The improper integral required was evaluated using the extended Simpson rule up to the maximum time point in the dataset and the remainder was evaluated as $\frac{i(\infty)}{s}$ where $i(\infty)$ is the steady-state current and *s* is the Laplace variable. The most significant source of error in the calculation of the Laplace transform was

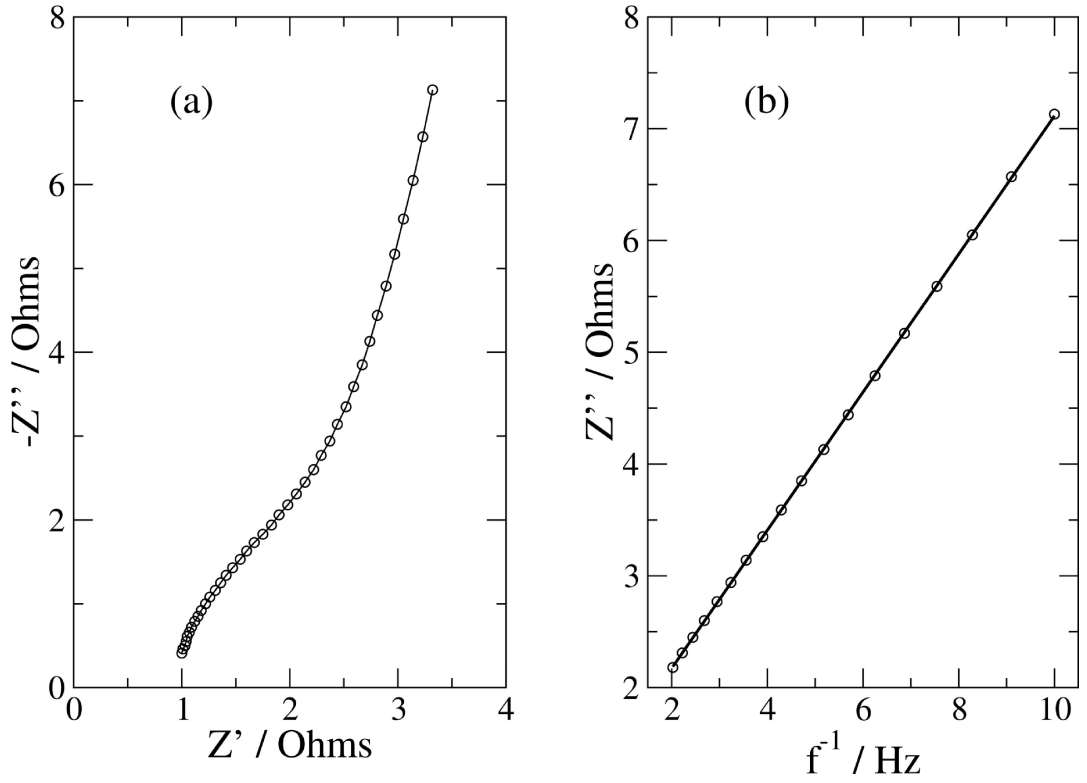

Figure 7. Impedance spectrum for a CO-AF sensor at the normal operating potential of 0.0 V in zero air. The frequency range was 0.1–10 Hz. (a) Nyquist plot of the impedance. (b) A plot of $-Z''$ against f^{-1} of the low frequency data, $f < 0.5$ Hz. The differential capacitance is 0.257 ± 0.00033 F.

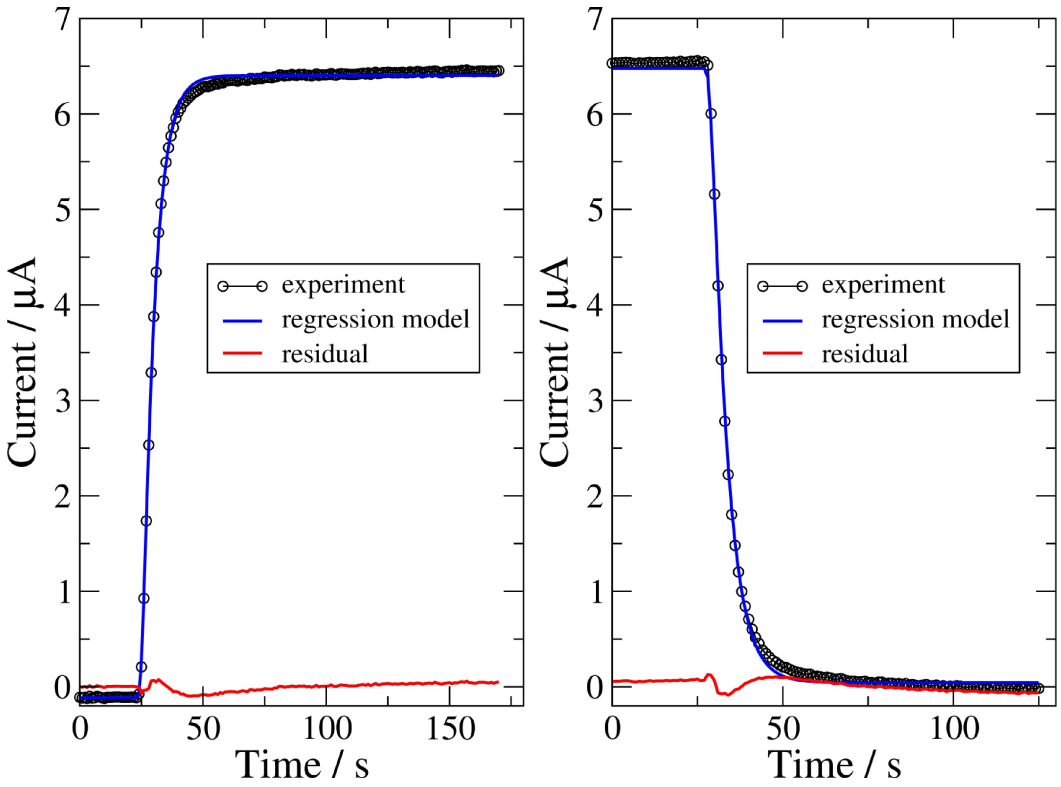

Figure 8. Data for the response of an amperometric CO-AF sensor to an abrupt change in CO concentration at a potential of 0.0 V and a temperature of 20 °C. (a) Response to gas-on at $t \simeq 22$ s. Chronoamperometric data for the response to a step from from 0–100 ppm CO in zero air, the fit of the regression model of Eq. (10) and the residual. The characteristic time obtained from the fit was $\tau = 47.3$ s. (b) Recovery after gas-off at $t \simeq 26$ s. Chronoamperometric data for the response to a step from from 100–0 ppm CO in zero air, the fit of the regression model of Eq. (10) and the residual. The characteristic time obtained from the fit was $\tau = 45.1$ s.

the choice of the origin, therefore the transform was applied to the data after determining the $t = 0$ point using the fit of Eq. (10). The transform acts to smooth the data and therefore the fit of Eq. (9) to the data shows more clearly the small deviations from the model in Figure 9 which are mainly a result of uncertainty in the background current at $t = 0$. In addition, the CO concentration at the outer surface (up to a constant factor of D/L) can be estimated directly from the data by multiplying the transformed data by $\sqrt{s}\sinh\sqrt{s}$ in Figure 9(c). The concentration – s data shows a horizontal line, indicating the concentration rises to a constant value at most a few seconds after the step, i.e. up to $s \simeq 0.2$. This is much less than the characteristic time of the sensor which gives confidence that the assumption of an abrupt concentration step is reasonable. At very short times, large s, the data deviates because a small error δt in setting the $t = 0$ point results in a factor of $e^{s\delta t}$ after Laplace transform.

Apart from the precision of the $t = 0$ estimate, the other limitation on short time data is the dead volume of the system. The flow rates used were ≥ 500 mL min^{-1} and the estimated "dead" volume (tubing + hood) was about 15 mL, which gives a dead time of ≤ 1.8 s. In order to study sensors with a much shorter τ than the CO-AF devices, the dead volume should be minimized by reducing the length of tubing between the gas mixing point and the sensor.

Previous workers have considered possible electrical limitations on the measured gas sensor response times.[18,30] In a potentiostatic experiment, these effects can arise because the applied potential is divided between the working electrode/solution interface, the reference electrode/solution interface and the solution resistance. There are three generic possibilities: either (i) the ohmic drop in the solution varies when a current flows in the presence of analyte, (ii) the presence of the analyte causes a small change in the interfacial capacitance of the working electrode, or (iii) a shift in the reference potential generates a charging current despite the diffusion-limited nature of the sensing reaction. In all cases, the uncompensated resistance R_u and the double layer capacitance C_{dl} control the time-dependence of the effect. The time constant can be estimated as $R_u C_{dl} \simeq 0.26$ s from the impedance data of Figure 7 and is much shorter than the measured response times in Figure 8. The electrical response of the cell therefore does not contribute significantly to the response time of the sensors studied here.

3.3. Effect of signal-to-noise ratio on estimates of the characteristic time

In typical operating conditions, the signal-to-noise ratio will be worse than during laboratory characterization of the sensor

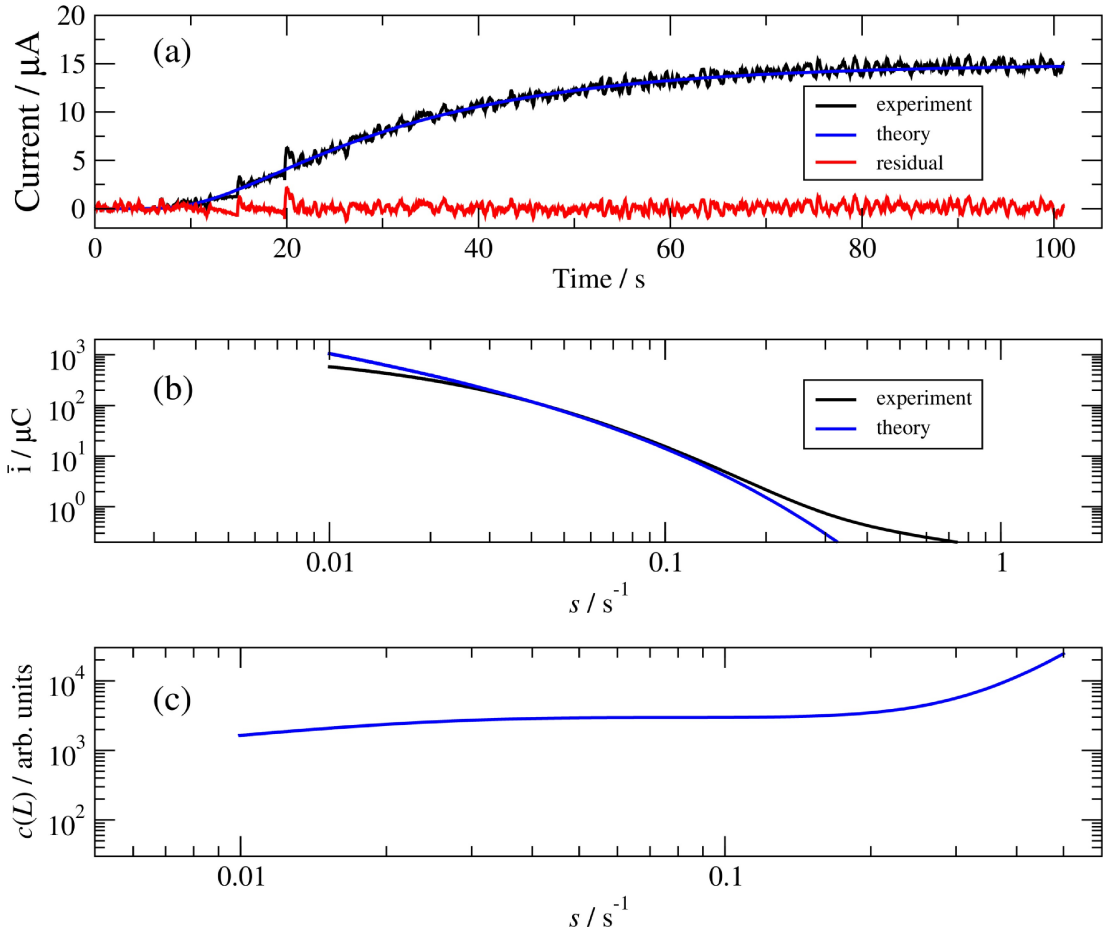

Figure 9. Typical data for the response of a CO-AF sensor to an abrupt change in CO concentration (0–200 ppm) at 0.0 V and the Laplace-transformed response. The Laplace parameter is *s*. (a) Chronoamperometric data, the fit of the regression model of Eq. (10) and the residual; (b) The Laplace-transformed current from (a) and the fit of Eq. (9) to the data; (c) Estimate of the concentration at the outer membrane using Eq. (9) and the data from part (b).

performance. We have investigated numerically the sensitivity of the estimated values of characteristic time to noise by the addition of Gaussian random deviates to the data of Figure 8. Two models of the noise are considered. In the first, Eq. (24), the noise is assumed proportional to the instantaneous vale of the current.

$$i_{sim}(t) = i_{expt}(t)[1 + \lambda\eta(t;\ 0,\ 1)] \tag{24}$$

The random variable $\eta(t;\ 0,\ 1)$ is a Gaussian deviate of zero mean and unit variance.[27] The dimensionless parameter λ controls the excess noise added to the experimental data i_{expt} to generate a simulated dataset i_{sim} in which the signal-to-noise ratio is λ^{-1} in so far as the noise in the experimental data can be neglected. The second model assumes the current noise is at a fixed level, which we take to be a fraction λ of the steady-state current as in Eq. (25).

$$i_{sim}(t) = i_{expt}(t) + \lambda\eta(t;\ 0,\ 1)i_{expt}(\infty) \tag{25}$$

Uncorrelated datasets of controlled signal-to-noise ratio were generated using Eqs. (24) and (25) using different seeds for the pseudo-random number generator and for a selection of values of λ in the range $0 < \lambda \leq 0.1$. Every simulated dataset was fitted to Eq. (10). The results are summarised in Figure 10.

As λ increases, the estimated characteristic time remains the same within the error bars under either noise model. This resilience of the model is simply related to the nature of least-squares fitting. However, the uncertainty of the fitted parameters becomes large when the signal to noise ratio decreases; the fractional error is of the order of λ in Figure 10(a) and larger in Figure 10(b). The standard errors from fits to individual datasets remain of the order of 0.5 s and are therefore poor estimates of uncertainty for large values of λ.

3.4. Temperature dependence of sensor behaviour

3.4.1. Transient response

Values of the effective thickness *L* and effective diffusion coefficient *D* were obtained from chronoamperometric concentration-step experiments for several CO sensors over the range −20 °C to +40 °C. As expected, the values of *L* were independent of temperature, but they were observed to depend on the porous membranes employed in the sensor

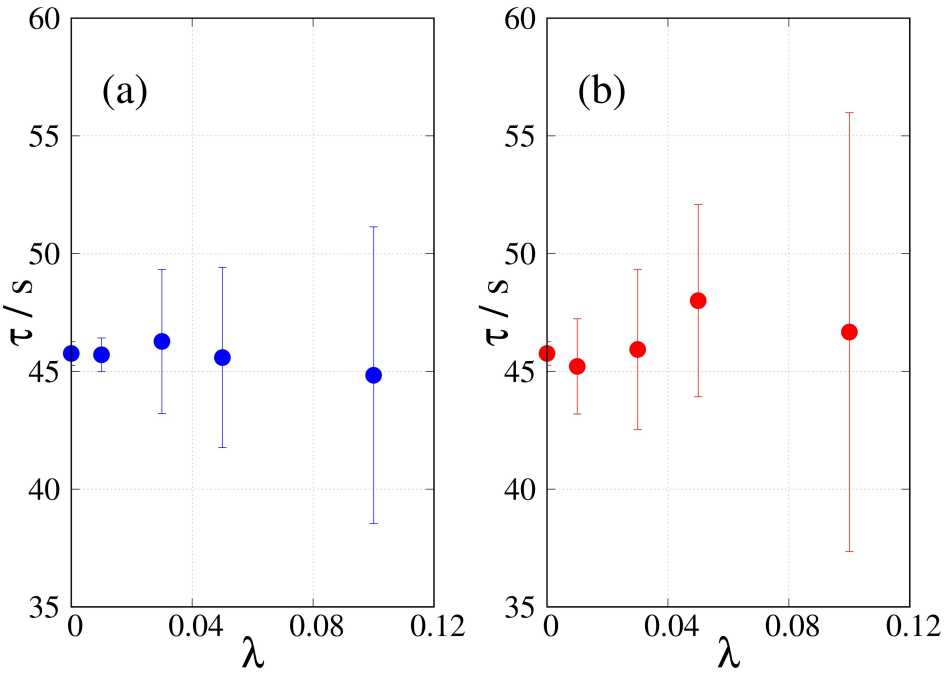

Figure 10. Effect of signal-to-noise ratio λ^{-1} on the characteristic time τ estimated from datasets simulated according to (a) Eq. (24) and (b) Eq. (25). For $\lambda = 0$, the error bar is a standard error estimated from the covariance matrix of the fit as 0.50 s. For $\lambda > 0$, the error bars are standard deviations obtained by analysing 10 simulated datasets.

construction. The standard design uses a Porex PTFE membrane of pore diameter 9–12 μm, porosity of 40–45% and a thickness of 0.18 mm. Some sensors were prepared using a thicker Gore PTFE membrane, which has a porosity of 20% and a thickness of 0.25 mm.

The effective thicknesses L are given in Table 1. The thicknesses are both of the order of 0.3 cm, which matches approximately the thickness of the filter layer in the device rather than the membrane itself. However, there is a significant difference between the effective thicknesses ($p = 0.019$) in a 1-tail unpaired t-test. This suggests that the effective thickness includes a contribution from both the membrane and the filter layer.

The D values were extracted by fitting Eq. (10) to chronoamperometric data at each temperature. We assumed $n = 2$ for the oxidation of CO and no kinetic limitations because the current transients were observed to be independent of potential over the range −0.1 V–+0.3 V which includes the normal dc operating potential of 0.0 V. The values of D are of the order of 10^{-3} cm^2 s^{-1} which is much greater than typical diffusion rates in aqueous media ($D \simeq 10^{-5}$ cm^2 s^{-1}) and lower than typical values in the gas phase ($D \simeq 10^{-1}$ cm^2 s^{-1}). If the rate-limiting step were simply diffusion in the electrolyte, then D/L in Eq. (10) would contain an extra factor of the Henry's law constant $H^{cc} \simeq 0.024$ at 298 K.[31] For a diffusion coefficient of order 10^{-5} cm^2 s^{-1}, the effective thickness in order to generate the observed τ would be $L \simeq 0.02$ cm and the sensitivity of the device would be only $\simeq 0.1$ nA ppm^{-1}, which is about 3 orders of magnitude smaller than experiment. The effective diffusion coefficient therefore represents an average over contributions from gas-phase and condensed-phase transport. Previous work estimated about a 70% contribution from diffusion in the electrolyte film by observing the effect of varying device parameters on the steady-state current.[20]

Figure 11 shows the variation of effective diffusion coefficients over the temperature range −20 °C to +40 °C. This also provides evidence of a gas-phase contribution in addition to diffusion in the electrolyte. An empirical correlation by Fuller, Schettler and Giddings[32] for a range of small molecule gases found that the diffusion coefficients vary with temperature as $T^{1.75}$. We find a similar power from our ln$D$ vs. ln$T$ data in Figure 11 for both standard, thick membrane (lower porosity, lower D) and without filter sensors. We note that this does not rule contributions from diffusion in the electrolyte (activated temperature dependence)[33] or Knudsen-type diffusion in the membrane,[25] because D is a composite value.

Table 1. Effective thicknesses L for the diffusion barriers in CO sensors prepared with standard and thick membranes. The values shown are mean and standard deviation for $n = 7$.

	L/cm
Standard	0.28 ± 0.032
Thick membrane	0.33 ± 0.036

3.5. Non-uniform accessibility

Careful examination of Figure 8 shows that the theoretical fit lies slightly above the data in the intermediate range of times. We observe this phenomenon in many, though not all, devices.

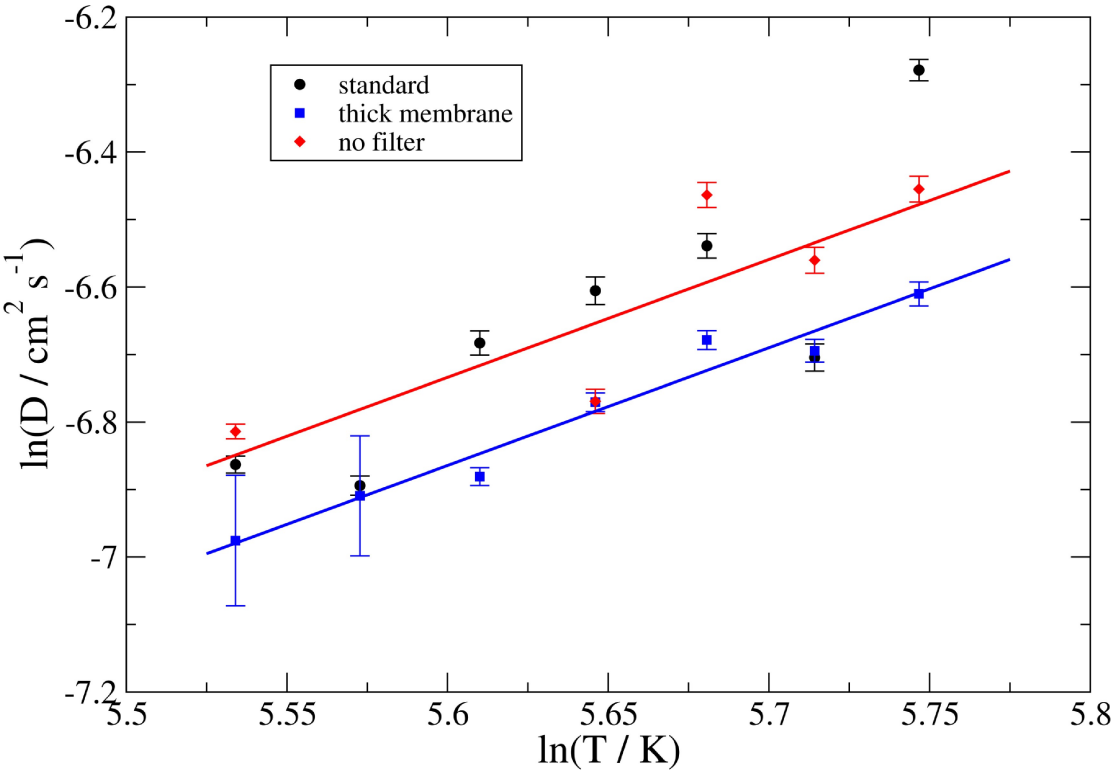

Figure 11. Effective diffusion coefficients for various sensors as a function of temperature. (black) standard membrane; (blue) thick membrane; (red) standard membrane, no filter. The data was obtained from the response of the sensors to a 0–400 ppm step in CO concentration over the temperature range −20 °C to +40 °C. The red and blue lines are linear regression of the standard and thick membrane data respectively. The slopes are 1.75 ± 0.40 and 1.74 ± 0.16.

It cannot be explained by a series of diffusion barriers because, as shown previously, that merely changes the effective L and D. We also show later in section 3.6 that it cannot be explained by kinetic limitations between layers in the device. However, it is possible that it is a result of non-uniformity in the device either inherent in the components or as a result of the manufacturing process. In general, L and D may vary across the device surface. This would produce a variation of current density across the electrode surface and a corresponding variation of τ across the device.

It is difficult to construct a general model for the case of non-uniform accessibility in amperometric gas sensors. However, an approximate approach can be made by treating the characteristic time $\tau = L^2/D$ as a random variable and computing the expected value of the current using the expression for a particular realization of τ from Eq. (10).

$$\frac{i}{i_\infty} = \int_\tau j'(t;\ \tau)p(\tau)d\tau \tag{26}$$

Where j' is the right-hand side of Eq. (10), but normalized so that $lim_{t\to\infty} j'(t) = 1$ and $p(\tau)$ is a probability density. j' can be computed easily by summing the series in Eq. (10) for a large number of terms and setting $j'(0) = 0$.

In order to use Eq. (26) as a regression model, the variable τ and the probability density $p(\tau)$ must be discretized (τ_i, p_{τ_i}) and it is necessary to enforce some smoothness constraints on p_{τ_i}. We chose to use a regularization in which the sum of squares of second order finite differences $\Sigma_i\left(\Delta^2 p_{\tau_i}\right)^2$ was minimized.

Figure 12 shows an example of this analysis applied to the response of a CO-AF sensor to 100 ppm CO in zero air. As noted above, the fit of Eq. (10) based on a single characteristic time τ and shown by the red curve, deviates positively from the data at intermediate times. In other words, the experimental data reaches the steady-state more slowly than predicted by the initial rise, which is well-described by Eq. (10). The blue curve shows the fit of the distributed model, Eq. (26), which describes the data well over the whole time range; parameters determined from the distributed model are collected in Table 2. The probability distribution of τ obtained from the fit of Figure 12(a) is shown in Figure 12(b); it can be approximated by a lognormal distribution plus a small contribution at large τ which is related

Table 2. Data for Figure 12.

T/°C	τ/s	τ_{mode}/s	σ/s
10, std	68.1	63.6	0.370
20, std	52.4	49.5	0.381
30, std	44.7	43.2	0.391
30, thick	70.9	67.7	0.372
30, nofiltr	47.1	43.9	0.366

std = standard device construction, thick = thicker membrane, nofiltr = filter omitted. σ is the standard deviation of a gaussian fit to the distribution of τ on a logarithmic scale.

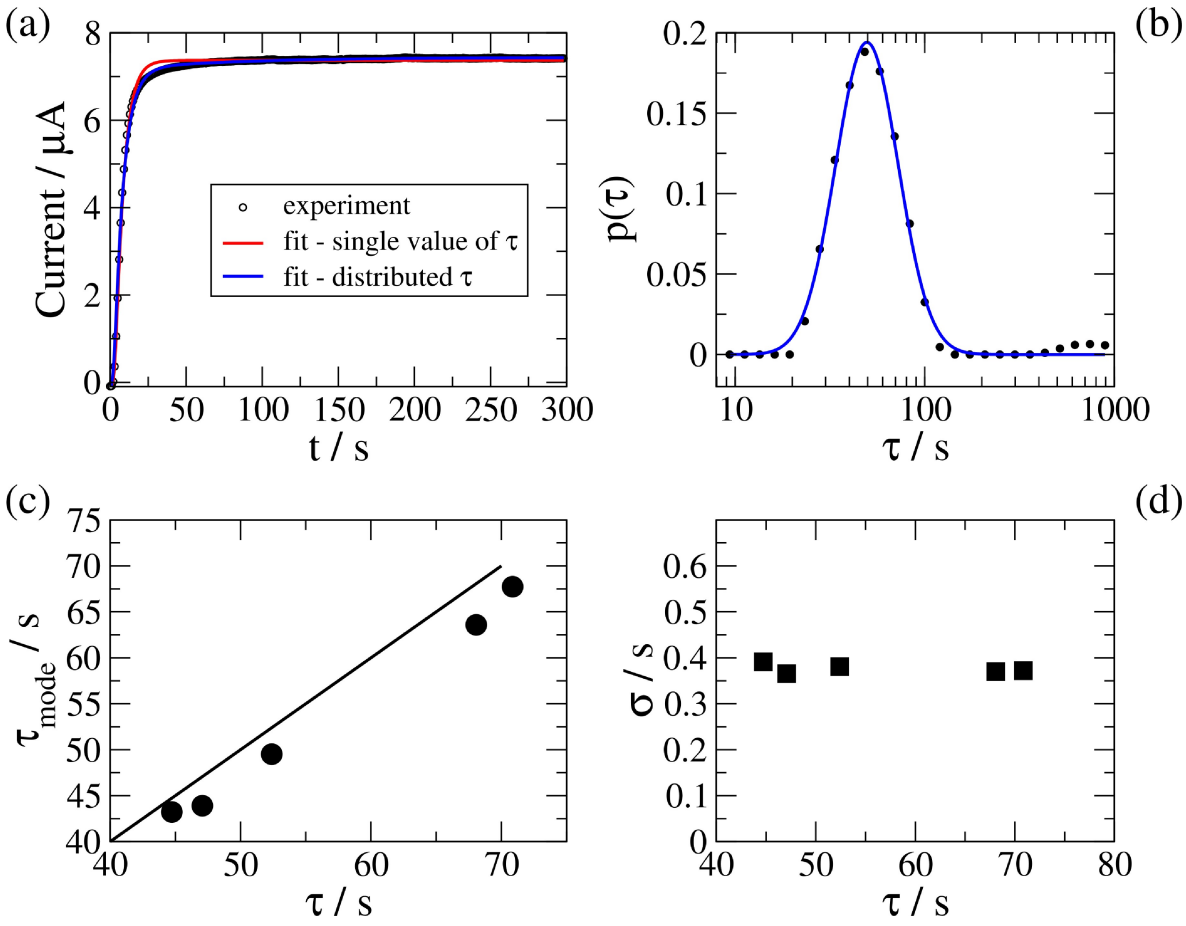

Figure 12. Fit of the regression model for a distribution of characteristic times, Eq. (26) and of Eq. (10) to chronoamperometric data for the response of a standard device to 100 ppm CO in zero air. (a) Experiment (symbols), Eq. (10) (red line) and Eq. (26) (blue line); (b) Distribution of characteristic times obtained from the fit of Eq. (26) in part (a) (symbols) and a lognormal distribution (blue line); (c) The modal values of characteristic time plotted against the single values obtained from fits to Eq. (10) for a dataset covering the range $T = 10\,°C$ to $+30\,°C$ for standard CO-AF devices, one device with a thick membrane, and one lacking the filter. The data is given in Table 2. (d) The standard deviations of the lognormal distributions for the data of part (c).

to the drift in the steady-state current. The modal values of characteristic time are close to the optimal values of the simple regression model of Eq. (10) as shown in Figure 12(c). Interestingly, the standard deviation σ is independent of temperature (Figure 12(d)) which suggests that it is related to a fixed property of the device such as the pore structure of the membrane/filter.

3.6. Interfacial kinetics

The potential-independence of the sensor response rules out a rate-limiting electrode kinetic step, however it does not rule out possible kinetic barriers at the various interfaces between different layers in Figure 1. For example, it is possible that there is a finite rate of dissolution of the analyte in the elecrolyte. This process is independent of electrode potential and therefore may limit the overall sensor current when the first order heterogeneous rate constant for dissolution of the analyte in the electrolyte is less than the mass transfer coefficient, $k \ll \frac{D}{L}$.

If we have a single diffusion barrier and a kinetic barrier at the outer surface, e.g., slow dissolution of the analyte gas in the electrolyte followed by diffusion through the electrolyte, then the chronoamperometric response can be calculated in the same way as Eq. (9) for diffusion only.

$$\overline{C_l} = A(s)\,\sinh\sqrt{s}X \tag{27}$$

Where X is a dimensionless coordinate normal to the electrode, defined as $X = \frac{z}{L}$. The dimensionless flux at the membrane surface is $J = \frac{L}{Dc^*} j = \left.\frac{\partial C_l}{\partial X}\right|_{X=1}$ and is given by the difference in the forward and backward dissolution rates, $k\bar{C}_g - \frac{k}{K}\bar{C}_l(1)$ so its Laplace transform is:

$$\bar{J} = \left.\frac{\partial \overline{C_l}}{\partial X}\right|_{X=1} = \frac{\mu}{s} - \frac{\mu}{K} A(s)\,\sinh\sqrt{s} \tag{28}$$

Where $\mu = \frac{kL}{D}$. The (Laplace-transformed) flux at the electrode surface is:

$$\bar{J} = \frac{K}{(K/\mu)s\,\cosh\sqrt{s} + \sqrt{s}\,\sinh\sqrt{s}} \tag{29}$$

As $\mu \to \infty$, and the kinetic barrier becomes less important, Eq. (29) tends to Eq. (9) as expected.

For the case where the dissolution kinetic limitation is at $X = 0$ and the electrode is covered by a thin film (inside the main diffusion barrier) and operated at the transport-controlled limit, so that the flux is $j = kc(0)$ and $J = \mu C(0)$ where, as before, $\mu = \frac{kL}{D}$,

$$\bar{J} = \frac{1}{(1/\mu)s\cosh\sqrt{s} + \sqrt{s}\sinh\sqrt{s}} \tag{30}$$

Eqs. (9), (29) and (30) show that slow interfacial kinetics does not affect the shape of the long-time (small s) region of the data because the ratio $\bar{j}/\bar{J}$ is independent of s as $s \to 0$. Fitting the experimental data to the regression model of Eq. (10) therefore gives values of τ that are only weakly affected by the interfacial kinetics as demonstrated in Figure 13. It is also worth noting that the sensor response is still well-modelled by Eq. (10) in the presence of such kinetic limitations and these effects cannot explain the behaviour attributed to the distribution of τ in the previous section.

The clear consequence of ignoring the possibility of slow kinetics in the analysis would be to underestimate the value of D/L because kinetic limitations do reduce the value of the steady-state current in Figure 13. In turn this would reduce the effective diffusion coefficient $D = \left(\frac{D}{L}\right)^2\tau$. In principle, evidence of kinetic limitations could be directly observed at short times, but this requires a precise knowledge of the dead volume of the system in order to obtain accurate data for large s.

4. Conclusions

The transient and steady-state response of amperometric gas sensors to an abrupt concentration step can be described by an effective thickness L and effective diffusion coefficient D. Analysis of these values provides insight into the rate-limiting steps of the devices under normal operating conditions. The method has the advantage that it is potentiostatic and charging currents do not interfer with the analysis. We find that under laboratory conditions, the dead volume of the system and the flow rate are such that the assumption of a sharp concentration step does not significantly affect the measured characteristic times $\tau = \frac{L^2}{D}$. As the signal-to-noise ratio decreases, the uncertainty in the estimated values of τ rises, but the mean of a series of replicates can tolerate Gaussian noise of at least a fraction 0.1 of the signal. For noisy data, an alternative method of analysis based on the same fundamental model can be performed conveniently after Laplace transformation of the data. The characteristic time τ obtained by fitting the data to the regression model of Eq. (10) can be used to characterise sensors with complex layered architectures. Alternately, if the behaviour of individual layers is known, Eqs. (22) and (23) can be used to predict sensor characteristics.

In Alphasense CO-AF devices, the temperature dependence and typical values of D suggest a contribution to the effective diffusion coefficient from gas-phase diffusion that is consistent with the Fuller–Schettler–Giddings empirical correlation $D \sim T^{1.75}$. Small deviations from the model are observed at

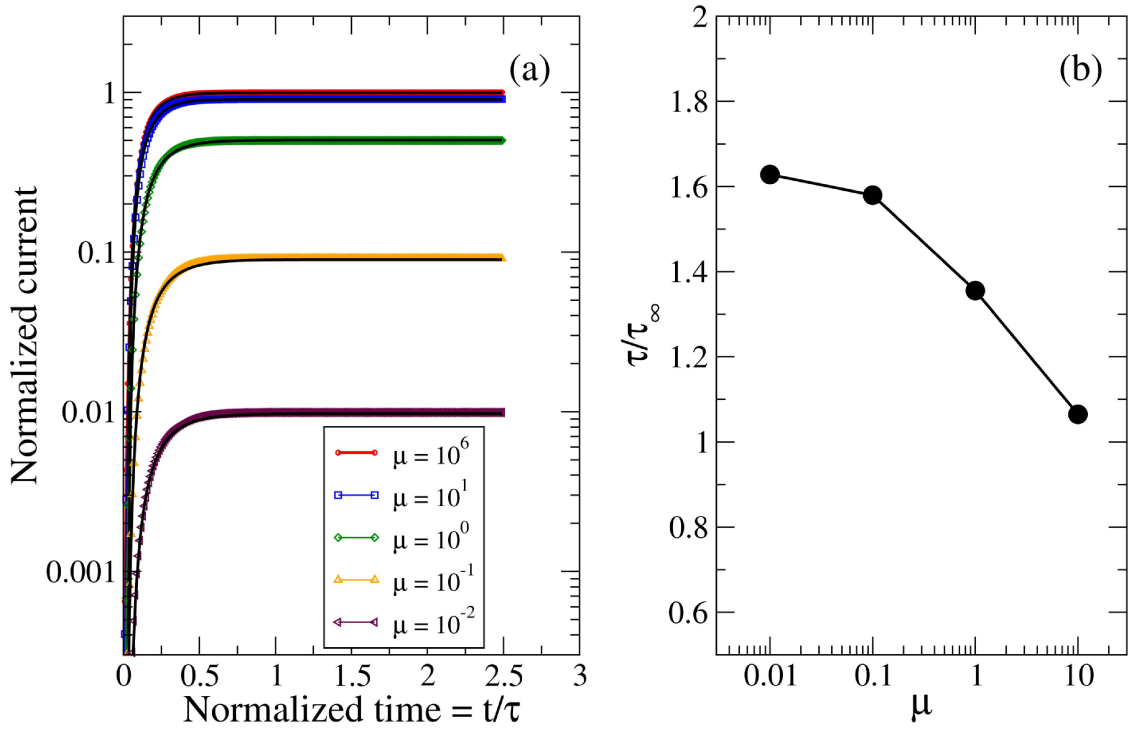

Figure 13. Effect of a kinetic barrier on the chronoamperometric response. (a) Simulated chronoamperometric responses to a concentration step (symbols) and the fit of the regression model (Eq. (10)) to the simulated data. The current is normalized to the steady state value for the case $\mu \to \infty$ and the time is normalized by the characteristic time τ for each curve. (b) Fitted values of the ratio of characteristic times τ/τ_∞ against the dimensionless rate constant $\left(\mu = \frac{kL}{D}\right)$. τ_∞ is the characteristic time in the absence of a kinetic barrier $(\mu \to \infty)$.

intermediate times but these can be understood on the basis of a distribution of characteristic times, with temperature-independent variance that arises from the structure of the device layers. The analysis shows that the model has wide applicability to complex electrode stacks, however there are two principal limitations: (i) short-time data ($t \ll \tau$) may be compromised by the dead volume of the system and/or the settling time of the mass flow controllers and (ii) it is difficult to detect the contribution of interfacial kinetic barriers, e.g., dissolution from gas to liquid phases, although the characteristic time $\tau = \frac{L^2}{D}$ obtained from the data in their presence remains approximately correct.

Conflict of Interests

The authors declare no conflict of interest.

Data Availability Statement

The data that support the findings of this study are openly available in data.ncl.ac.uk at https://doi.org/10.25405/data.ncl.24552007, reference number 24552007.

Keywords: Gas sensors · amperometry · diffusion · simulation

[1] R. Baron, J. R. Saffell, *ACS Sens.* **2017**, *2*, 1553–1566.
[2] Z. Cao, W. J. Buttner, J. R. Stetter, *Electroanalysis* **1992**, *4*, 253–266.
[3] M. I. Mead, O. A. M. Popoola, G. B. Stewart, P. Landshoff, M. Calleja, M. Hayes, J. J. Baldovi, M. W. McLeod, T. F. Hodgson, J. Dicks, A. Lewis, J. Cohen, R. Baron, J. R. Saffell, R. L. Jones, *Atmos. Environ.* **2013**, *70*, 186–203.
[4] M. Hossain, J. R. Saffell, R. Baron, *ACS Sens.* **2016**, *1*, 1291–1294.
[5] M. Dmitrzak, P. Jasinski, G. Jasinski, *Bull. Pol. Acad. Sci. Tech. Sci.* **2020**, *68* (6), 1275–1282.
[6] A. W. E. Hodgson, P. Jacquinot, L. R. Jordon, P. C. Hauser, *Anal. Chim. Acta* **1999**, *393* (1–3), 43–48.
[7] L. Xiong, R. G. Compton, *Int. J. Electrochem. Sci.* **2014**, *9*, 7152–7181.
[8] S. Das, V. Jayaraman, *Prog. Mater. Sci.* **2014**, *66*, 112–255.
[9] T. Villa, F. Salimi, K. Morton, L. Morawska, F. Gonzalez, *Sensors* **2016**, *16*, 2202.
[10] S. C. Chang, J. R. Stetter, S. C. Cha, *Talanta* **1993**, *40*, 461–477.
[11] J. Chou, *Hazardous gas monitors. A practical guide to selection, operation and applications.* McGraw-Hill: New York, **2000**.
[12] J. R. Stetter, J. Li, *Chem. Rev.* **2008**, *108*, 352–366.
[13] M. Dmitrzak, P. Kalinowski, P. Jasinski, G. Jasinski, *Sens. Rev.* **2022**, *42* (2), 195–203.
[14] L. C. Clark, R. Wolf, D. Granger, Z. Taylor, *J. Appl. Physiol.* **1953**, *6* (3), 189–193.
[15] C. E. W. Hahn, *Analyst* **1998**, *123* (6), 57–86.
[16] Alphasense Ltd. Application note AAN 104, How Electrochemical Gas Sensors Work. Technical report, https://www.alphasense.com/, **2022**.
[17] J. Gebicki, B. Chachulski, *Electroanalysis* **2009**, *21*, 1568–1576.
[18] P. R. Warburton, M. P. Pagano, R. Hoover, M. Logman, K. Crytzer, Y. J. Warburton, *Anal. Chem.* **1998**, *70*, 998–1006.
[19] F. G. Cottrell, *Z. Phys. Chem.* **1903**, *42*, 385.
[20] M. L. Hitchman, N. J. Cade, T. K. Gibbs, N. J. M. Hedley, *Analyst* **1997**, *122*, 1411–1417.
[21] V. P. Chviruk, V. A. Nedashkovskii, O. V. Linyucheva, A. I. Buket, *Russ. J. Electrochem.* **2006**, *42* (1), 71–80.
[22] P. Sedlak, P. Kubersky, P. Skarvada, A. Hamacek, V. Sedlakova, J. Majzner, S. Nesurek, J. Sikula, *Metrol. Meas. Syst.* **2016**, *23*, 531–543.
[23] Alphasense Ltd. Datasheet CO-AF carbon monoxide sensor. Technical report, https://www.alphasense.com/, **2022**.
[24] M. L. Hitchman, *Measurement of dissolved oxygen.* Chemical analysis. Wiley, New York, **1978**.
[25] C. Xia, X. Lu, Y. Yan, T. Wang, Z. Zhang, *Sens. Actuators B* **2011**, *156* (2), 881–886.
[26] J. Crank, *The mathematics of diffusion.* Clarendon Press, Oxford, reprinted edition, **1970**.
[27] W. H. Press, S. A. Teukolsky, W. T. Vetterling, B. P. Flannery, *Numerical Recipes in Fortran; The Art of Scientific Computing, 2nd ed.;.* Cambridge University Press: Cambridge, UK, **1992**.
[28] R. de Levie, *Electrochim. Acta* **1964**, *9*, 1231–1245.
[29] J. P. Meyers, M. Doyle, R. M. Darling, J. Newman, *J. Electrochem. Soc.* **2000**, *147*, 2930–2940.
[30] J. Lu, S. Gong, H. Yan, J. Yang, *Electroanalysis* **1999**, *11* (4), 249–253.
[31] R. Sander, *Atmos. Chem. Phys.* **2015**, *15*, 4399–4981.
[32] E. N. Fuller, P. D. Schettler, J. C. Giddings, *Ind. Eng. Chem.* **1966**, *58*, 19–27.
[33] D. L. Wise, G. Houghton, *Chem. Eng. Sci.* **1968**, *23*, 1211–1216.

Manuscript received: November 24, 2023
Revised manuscript received: January 12, 2024
Version of record online: ■■, ■■

RESEARCH ARTICLE

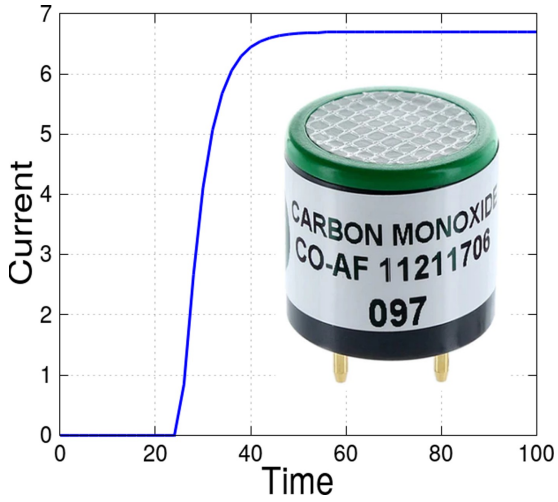

*L. Saunders, L. K. Mudashiru, R. Baron, B. R. Horrocks**

Diffusion models for the response of commercial amperometric gas sensors to a concentration step of the analyte are analysed. Effective values of barrier thickness and diffusion coefficient can be extracted for devices with complex layered architectures and possible interfacial phase transfer barriers. Small deviations of the experimental data from the model reflect a distribution of diffusivities in the devices.